

## Article

# Doped Potassium Jarosite: Synthesis, Characterization and Evaluation as Biomaterial for Its Application in Bone Tissue Engineering

Juan R. Serralde-Lealba <sup>1</sup>, Eduardo Cerecedo-Sáenz <sup>1</sup>, Juan Hernández-Ávila <sup>1</sup>, Alberto Arenas-Flores <sup>1</sup>,  
María A. Veloz-Rodríguez <sup>1</sup>, María del P. Gutiérrez-Amador <sup>2</sup>, Arelly M. González-González <sup>3</sup>,  
Raúl Rosales-Ibáñez <sup>3,\*</sup> and Eleazar Salinas-Rodríguez <sup>1,\*</sup>

- <sup>1</sup> Academic Area of Earth Sciences and Materials, Institute of Basic Sciences and Engineering, Autonomous University of the State of Hidalgo, Highway Pachuca-Tulancingo km. 4.5, Mineral de la Reforma 42184, Mexico; jurusele@gmail.com (J.R.S.-L.); mardenjazz@yahoo.com.mx (E.C.-S.); herjuan@uaeh.edu.mx (J.H.-Á.); arenasa@uaeh.edu.mx (A.A.-F.); mveloz@uaeh.edu.mx (M.A.V.-R.)
- <sup>2</sup> Apan High School, Autonomous University of the State of Hidalgo, Highway Apan-Calpulalpan km. 8, Apan 43920, Mexico; gutierrezam@yahoo.com
- <sup>3</sup> Tissue Engineering and Translational Medicine Laboratory, Faculty of Higher Education, Iztacala, National Autonomous University of Mexico, Tenayuca-Chalmita S/N, Cuauhtepac, Barrio Bajo, Alcaldía Gustavo A. Madero, Ciudad de México 07239, Mexico; arely.gonzalez@iztacala.unam.mx
- \* Correspondence: rosales\_ibanez@unam.mx (R.R.-I.); salinasr@uaeh.edu.mx (E.S.-R.); Tel.: +52-444-803-8048 (R.R.-I.); +52-771-207-4171 (E.S.-R.)



**Citation:** Serralde-Lealba, J.R.; Cerecedo-Sáenz, E.; Hernández-Ávila, J.; Arenas-Flores, A.; Veloz-Rodríguez, M.A.; Gutiérrez-Amador, M.d.P.; González-González, A.M.; Rosales-Ibáñez, R.; Salinas-Rodríguez, E. Doped Potassium Jarosite: Synthesis, Characterization and Evaluation as Biomaterial for Its Application in Bone Tissue Engineering. *Metals* **2022**, *12*, 1052. <https://doi.org/10.3390/met12061052>

Academic Editor: Srecko Stopic

Received: 29 April 2022

Accepted: 15 June 2022

Published: 20 June 2022

**Publisher's Note:** MDPI stays neutral with regard to jurisdictional claims in published maps and institutional affiliations.



**Copyright:** © 2022 by the authors. Licensee MDPI, Basel, Switzerland. This article is an open access article distributed under the terms and conditions of the Creative Commons Attribution (CC BY) license (<https://creativecommons.org/licenses/by/4.0/>).

**Abstract:** For decades, jarosites have been precipitated by controlling Fe in hydrometallurgical circuits. In addition, their synthesis, characterization, precious metals incorporation, decomposition and leaching have led to important results in this field. Nowadays, new topics related to the synthesis of these compounds have directed studies for applications such as lithium-ion batteries (as cathodes or/and anodes). Additionally, in this work, the evaluation of these kinds of compounds as biomaterials to be used in bone tissue engineering is shown, which is a novel application of these jarosite type-compounds. The method used for the synthesis of these compounds has been improved, decreasing the temperature (from 95 to 70 °C) and synthesis time (from 24 to only 3 h), which allows the doping of the potassium jarosite with calcium, strontium and magnesium (JKCa, JKCa<sub>2</sub> and JKAl). The powders obtained this way were characterized confirming the incorporation of these elements into the structure, and the biological assays allowing the cell proliferation at 10 days conclude that these compounds are viable as a biomaterial, due to their non-toxic property. On the other hand, these jarosites show osteoinduction when added to the swine dental pulp stem cells and can be used for orthodontic purposes.

**Keywords:** potassium jarosite; synthesis; biomaterial; bone tissue engineering; cells proliferation; osteoinduction

## 1. Introduction

The jarosite-type compounds, represented by  $MFe_3(SO_4)_2(OH)_6$  where M can be Na, K, Rb, Ag or  $NH_4$ , have had a wide application in metallurgical and mineralogical processes [1–5]. Figure 1 shows a natural jarosite crystal [6] contrasted with the crystals obtained using the synthesis conditions similar to those shown in this paper [7]. They are often associated with acid-mine drainage, weathering of sulfide ore deposits, hydrothermal alterations, oxidation of pyrite or weathering in acid soils [8]. They even occur in naturally acidic saline sediments under oxidizing conditions and low values of pH [9], which can occur in two types of settings: the first type is the volcanic one, where gases including  $H_2S$  and  $SO_2$  are dissolved and oxidized in caldera lakes or hot springs [10]; while the second type is present in areas where iron sulfide minerals are oxidized [11].

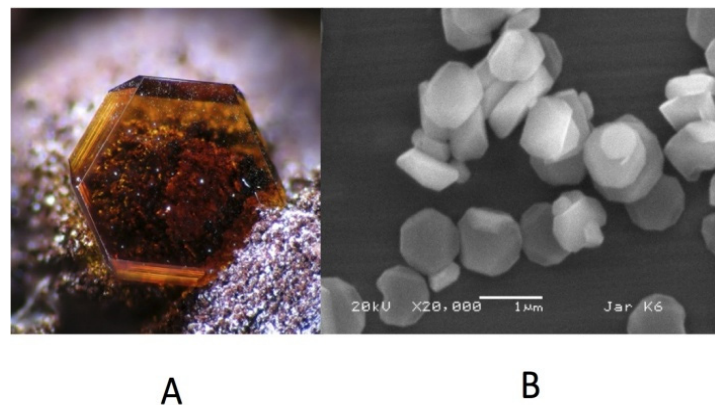


**Figure 1.** (A). A natural crystal of jarosite-type compound [6], and (B). Crystals of potassium jarosite obtained with the synthetic method described in this work [7].

The potassium jarosite with formula  $\text{KFe}_3(\text{SO}_4)_2(\text{OH})_6$  and whose mineral name is simply jarosite [1,12], has been employed in the zinc industry process to precipitate non-desired iron and other elements to facilitate the filtering stage [7,13]. Additionally, the recovery of valuable metals from jarosite residues has been addressed [14–16]. However, some investigations have mentioned the use of this type of compound as anodes and/or cathodes in lithium-ion batteries, through the synthesis of a two-dimensional material composed by  $\text{KFe}_3(\text{SO}_4)_2(\text{OH})_6/\text{rGO}$  using graphene oxide sheets through an oxidation process in the solution phase at an elevated temperature [7,17]. Recent studies have proven that there may be an electrochemical ion exchange in jarosite, with structurally stable mixed phases existing [18]. Therefore, by doping this kind of material with some elements such as calcium sulfate [19], it could be a promising strategy to overcome the shortage of grafts suitable for bone healing in tissue regeneration, due to its properties and good compatibility [20].

All the studies related to jarosite-type compounds have found interesting and advanced innovation, either modifying parameters and synthesis methods, or obtaining appropriate morphologies and particle sizes to evaluate new properties that place them as a material with possible applications in new fields such as that of bone tissue engineering.

The above is based mainly on three fundamental components: cells, scaffolds (biomaterials) and biomolecules, or inducers of growth factors [21]. Ideally, the combination of these three elements creates a surgically transplantable product that promotes bone tissue regeneration and restores the intrinsic biological function of bone tissue [22]. Most of the biomaterials used as scaffolds in the creation of an extracellular matrix (ECM) are made with calcium silicate ceramics [23], calcium phosphate [24] or strontium-based bioactive ceramics [25], whose evidence indicates that they promote enhanced bone repair and radiopacity for easy imaging. In addition, another researcher [26] reported the effects and mechanisms of strontium-promoted osteogenic differentiation of the mesenchymal stem cell. The fields of tissue engineering and regenerative medicine continue to face grueling challenges because of the difficulty of recreating the inherent complexity of the regenerative milieu [27].

Therefore, this work demonstrates improvements in the synthesis method of the doped potassium jarosite, such as a low operating temperature ( $70^\circ\text{C}$ ), doping with calcium, short synthesis time (3 h) and changes in pH. Therefore, this modified method [7] makes the synthesis of these kind of compounds economical and environmentally friendly. In this manner, the addition of other elements into the jarosite structure and the changes proposed in the synthesis pH values have contributed significantly to the final morphology and the size of particles of potassium jarosite obtained.

The osteoinductive property of jarosite without adding an osteoinductor differentiation medium, signaling to produce bone proteins, due to its intrinsic characteristics is acting as an inductor. Finally, the obtained product could be an ideal novel material to be

used for bone tissue engineering, according to its good osteoinductive properties and biocompatibility, which will be proven with the corresponding cytotoxic analysis.

## 2. Materials and Methods

### 2.1. Synthesis of the Doped Potassium Jarosite

In the present work, the synthesis method used was the same as that published by other researchers [7], which is a modified version of that reported by other authors years before [1,12,15]. The used method, here, reduces significantly the reaction time from 24 to only 3 h, the working temperature from 97 to 70 °C and variations in the pH and the concentrations of the precursors. The synthesis of the jarosite-type compounds used in this work was carried out under the following conditions: 0.15 M of  $\text{Fe}_2(\text{SO}_4)_3 \cdot n\text{H}_2\text{O}$  (J.T. Baker, Phillipsburg, NJ, USA), 0.15 M of  $\text{K}_2\text{SO}_4$  (J.T. Baker, Phillipsburg, NJ, USA) and 0.03 M of the corresponding element that doped the jarosite, in sulfate form ( $\text{CaSO}_4 \cdot n\text{H}_2\text{O}$  (Técnica Química S.A., Mexico City),  $\text{SrSO}_4$  (Aldrich Chemical Company, Inc. Milwaukee, WI, USA) or  $\text{MgSO}_4 \cdot 7\text{H}_2\text{O}$  (Meyer, Mexico City)). The aqueous solution was prepared in a 1.0 L three-neck flask with deionized water, and equipped with a pH measurement system, with the temperature maintained at 70 °C and mechanical stirring. Figure 2 shows the experimental array described. Additionally, all chemicals described and also the sodium hydroxide (NaOH) and sulfuric acid ( $\text{H}_2\text{SO}_4$ ) used for adjusting pH, were purchased from Sigma-Aldrich (St. Louis, MO, USA) with high purity (>99%).

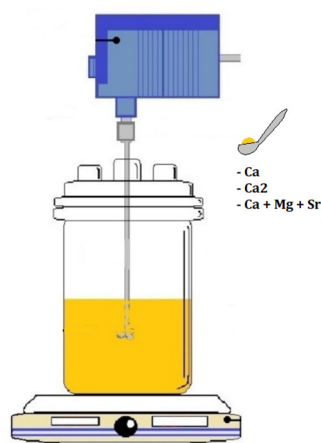


**Figure 2.** Experimental setup for the synthesis of doped jarosite-type compounds, pH 1.7, 70 °C, 500 rpm.

Finally, once the synthesis reaction finished, the solution remained at rest for a preset time to avoid particles coalescence, and then the solid product was leached with abundant hot deionized water (>60 °C) to eliminate residual sulfates. After this, the product was filtered, dried and characterized.

### 2.2. Chemical and Mineralogical Characterization of Synthesis Product

Regarding the protocols used for the analytical techniques used for the characterization of solids, samples were prepared by sieving to reach particle sizes lower than 75  $\mu\text{m}$ , and then were dried at 100 °C during 6 h in a lab oven with digital control. The analysis method used for the characterization was the following: X-ray diffraction using an INEL Diffractometer model Equinox 2000 located at the Autonomous University of the State of Hidalgo (AUSH), Mexico and manufactured by INEL at Artenary, Centre Val de Loire, France. The sweep time was 0.5 min for each sample, and the indexing of the obtained diffractograms was carried out with the MATCH version 1.1 software (developed by Crystal Impact, Bonn, Germany).

On the other hand, the morphological study conducted on samples was executed using a JEOL Scanning Electron Microscope JSM-IT300, manufactured by JEOL Tokyo,

Japan (located at the AUSH), using an operating voltage of 30 keV and equipped with an Oxford energy dispersive spectrometry (EDS).

Finally, to complete and confirm the presence of the doped elements into the jarosite structure, a total reflectance Fourier transform infrared (ATR-IFTR) examination was executed. It was completed using a Perkin Elmer Frontier FTIR spectrometer (Waltham, MA, USA), and 10 mg of the powdered sample was carefully placed on the crystal surface and each obtained spectrum was recorded as absorbance under 75%. Each spectrum was scanned between 4000 and 400  $\text{cm}^{-1}$  wavelengths.

### 2.3. MTT Assay

The 3-(4,5-dimethylthiazol-2-yl)-2, 5-diphenyltetrazolium bromide (MTT) colorimetric cellular metabolic assay was used to measure the possible cytotoxic effect of doped potassium jarosite on swine dental pulp stem cells (SDPSCs), based on the conversion of MTT into formazan crystals by living cells (which are primary cell cultures taken directly from the animal in the laboratory), which determines mitochondrial activity [28]. The cells were seeded in 96-well plates at a density of 4000 cells/well, and cultured in the medium. Jarosite samples were added after 24 h with a volume of 7  $\text{mm}^3$  per well. In all cases, and cultured in low-glucose DMEM (Bio-west, Mexico City), 10% of Fetal Bovine Serum (FBS) (Bio-west, Mexico City) and 1% penicillin-streptomycin (Sigma Aldrich, St. Louis, MO, USA), incubated at 24 h at 37 °C, 5%  $\text{CO}_2$ , after 24 h jarosite were added (cell seeded alone in the well, as a control group). The experiment was completed in triplicate, and the well-plates were incubated at different times: 3, 7 and 10 days at 37 °C, 5%  $\text{CO}_2$ . Then at each time, the cells were incubated with a solution of 10% MTT for 4 h at 37 °C protected from light. Finally, isopropanol was added to solubilize the formazan salts. Metabolic activity was measured by an Elisa plate reader (Biotek Elx808, USA) equipped with a 562–630 nm filter.

### 2.4. Osteogenic Differentiation and Calcium Deposits Evaluated by Alizarin Red Staining

Cells were seeded at a density of 5000 cell of DPSCs on 24 well-plates and cultivated with low-glucose DMEM (Bio-west, Mexico City), supplemented with 10% Fetal Bovine Serum (FBS) (Bio-west, Mexico City) and 1% penicillin-streptomycin (Sigma Aldrich, St. Louis, MO, USA), and incubated at 37 °C, 5%  $\text{CO}_2$  under humidification for 24 h. After that time, they were evaluated in three groups as explained below: cells in the well alone cultured with low-glucose DMEM (Bio-west, Mexico City), supplemented with 10% Fetal Bovine Serum (FBS) (Bio-west, Mexico) and 1% penicillin-streptomycin (Sigma Aldrich, St. Louis, MO, USA) (group A); cells and jarosite (10  $\text{mm}^3$ /well) and low-glucose DMEM (Bio-west, Mexico City), supplemented with 10% Fetal Bovine Serum (FBS) (Bio-west, Mexico City) and 1% penicillin-streptomycin (Sigma Aldrich, St. Louis, MO, USA) (group B); and cells, jarosite and MesenCult™ Osteogenic Differentiation Medium (consisting of basal medium, 15  $\mu\text{L}$  dexamethasone, 250  $\mu\text{L}$  ascorbic acid, 175  $\mu\text{L}$   $\beta$ -glycerophosphate and 7.5 mL MesenCult™ Osteogenic Stimulating Supplement (Stem Cells Technologies, Cambridge, MA, USA) (group C). All plates were incubated at 37 °C, 5%  $\text{CO}_2$  under humidification and the culture medium was changed once a week for 28 days. After these days, the evaluation of the osteogenic differentiation of the DPSCs mediated by the jarosite was carried out, with the Alizarin red staining (ARS) (Sigma Aldrich, St. Louis, MO, USA) colored calcium deposits selectively, and it has been used for decades to evaluate calcium-rich deposits in cell culture [29]. The culture medium was removed from the well-plate, and then the cells were fixed 20 min with 3.74% neutral formalin (Sigma Aldrich, St. Louis, MO, USA) for 5 min. Furthermore, they were washed three times with phosphate buffered saline (Bio-west, Mexico City), and further washed with distilled water in order to remove any salt residues. A solution of 2% wt/v ARS, with adjusted pH 4.2 was added, so that it covered the entire surface of the jarosite. After 60 min of incubation at room temperature, the ARS excess was washed with water. The ARS staining was imaged using a Leica DM

IL LED inverted light-field phase contrast optical microscope. All the experiments were performed in triplicate.

### 3. Results

#### 3.1. Synthesis of the Doped Potassium Jarosite

Three jarosite samples were obtained, named JKCa for the calcium doped jarosite, JKCa2 for the calcium doped jarosite twice the calcium, and JKAll for the jarosite doped with calcium, strontium and magnesium, and are shown in Figure 3. Once synthesized, the corresponding pH was measured using a pH meter (Dual Star PH/ISE with electrode and probe ATC brand Thermo Orion, manufactured by ThermoFisher Scientific, Waltham, MA, USA), obtaining values of 3, 3.5 and 3.2, respectively. According to these results, samples were washed using deionized water at a boiling temperature under mechanical stirring and adding to the rest of the solution during 2 to 3 min, and finally filtered to get the samples to be dried. The washing process was completed twice, and again pH was measured until values of 6.9 for JKCa, 7.2 for JKCa2 and 7.4 for JKAll were obtained, which are acceptable to be used in cell assays [30].



**Figure 3.** Samples of doped jarosite-type compounds obtained after synthesis.

#### 3.2. Characterization of Synthesized Jarosites

Scanning electron microscopy (SEM) in conjunction with the energy dispersive spectrometry of X-ray (EDS) were used to evaluate the morphological and compositional properties of the doped jarosite powders obtained, in order to interpret their relationship with the structural properties and corroborate the adequate incorporation of doped elements into the corresponding structure. Figure 4a shows the SEM-SE image for the JKCa where the spherical agglomerate particles corresponding to the potassium jarosite can be seen, which are quite similar to those obtained in a previous work [7], with particle sizes varying from 1 to 10  $\mu\text{m}$ . Some groups of agglomerated particles show a linear growing pattern on a calcium cylinder such as that observed in Figure 4a,b, which corresponds to the JKCa2 sample. Similarly, the element distribution involved in these samples can be appreciated in Figure 5a,b.

For the case of the JKAll sample, it can be observed (Figure 4c) that there are small particles ( $\sim 1 \mu\text{m}$ ) and agglomerates of sizes up to 15  $\mu\text{m}$ , having an average size of 7  $\mu\text{m}$ . In addition, it can be noticed that the presence of great particles containing Sr, Mg and Ca in a not rounded morphology could represent a new phase, along with jarosite particles giving a mixture of two solid solutions. In the same way, in this image the presence of calcium, strontium and magnesium distributed in such particles as is shown in Figure 5c, could be observed.

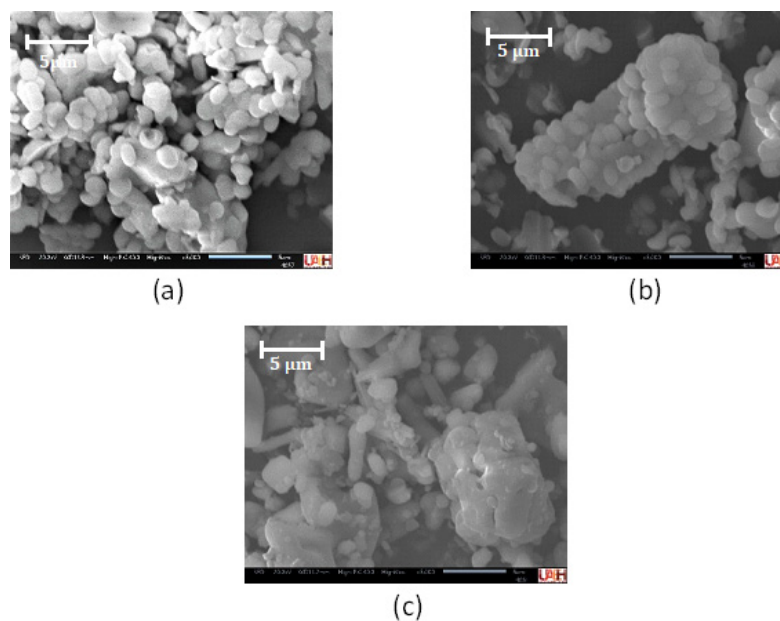


**Figure 4.** SEM (SE) images of doped jarosite-type compounds: (a) JKCa; (b) JKCa2; and (c) JKAl.

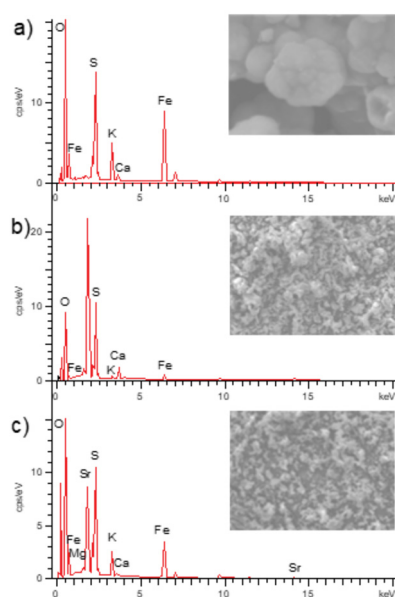


**Figure 5.** EDS (SEM) spectra showing the semi-quantitative chemical composition for the doped jarosite-type compounds: (a) JKCa; (b) JKCa2; and (c) JKAl.

Figure 4b shows the JKCa2, where the change of structure of jarosite observing shapes that are no longer so rounded, but elongated with some bright spots that correspond to the calcium in the structure (Table 1) can be appreciated. The above can also be observed in Figure 5b.

**Table 1.** Semi-quantitative chemical composition by energy dispersive spectrometry analysis in jarosite samples (weight percentage, % wt).

Jarosite \ Element	O	S	K	Fe	Ca	Sr	Mg	Total
JKCa	48.85	12.67	5.96	35.10	0.43	-	-	100
JKCa2	64.45	24.00	0.79	6.08	4.67	-	-	100
JKAl	51.09	13.08	3.65	15.76	0.17	16.19	0.06	100

In the case of JKAll, it can be observed (Figure 4c) that there is a change in the morphology which could be due to a change in the crystalline structure. In this figure, smaller particles ( $\sim 1 \mu\text{m}$ ) can also be observed and crowds bigger than  $10 \mu\text{m}$ , with an average particle size of  $7 \mu\text{m}$ . Similarly, in the image it can be observed that bright spots which could be due to the presence of calcium, strontium and magnesium, are incorporated into the jarosite structure as shown in Figure 5c.

According to the obtained results executed by ATR-FTIR, more information was obtained related to the chemical composition of samples regarding the incorporation or not of the doped elements. Shifts in the frequency of absorption bands and relative band intensities, indicate changes in the structure or changes in the surroundings of the samples [31]. Through the electromagnetic radiation, the IR region spreads from 10 to  $13,000 \text{ cm}^{-1}$  and only the mid-IR region ( $400\text{--}4000 \text{ cm}^{-1}$ ) is utilized in the conventional IR analysis, because fundamental vibration or functional groups which are subject to analysis, belong to this region [32].

Figure 6 depicts IR spectra of three samples and a potassium jarosite control. It can be observed that the IR spectra of JKCa and JKCa2 are very similar to the potassium jarosite.

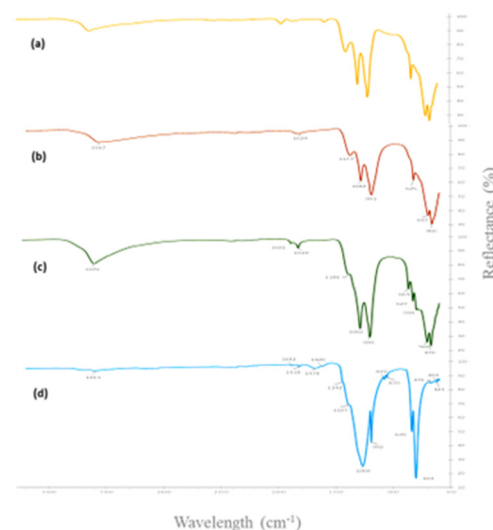


**Figure 6.** FTIR spectra of: (a) potassium jarosite, (b) JKCa, (c) JKCa2 and (d) JKAll.

According to the above, for the case of JKCa and JKCa2, both exhibit absorption bands having comparable shapes and positions, and only a few peaks of calcium sulfate appear near  $590$ ,  $660$  and  $1600 \text{ cm}^{-1}$  [33]. On the other hand, JKAll shows a typical spectrum of the strontium sulfate [34]. Figure 7a shows just one band, which is primarily due to the structural OH stretching mode and includes water modes, especially for the synthetic samples. Reflectance spectra in this region are nearly saturated for these sulfates [35].

The spectral features seen in the three jarosites arise from the S-O bond oscillations of the sulfate anion at approximately  $1100\text{--}1200 \text{ cm}^{-1}$  [36] due to asymmetric stretching (Figure 7b). In addition, the  $680$  and  $600 \text{ cm}^{-1}$  features are both components of the normal mode of vibration [37] (Figure 7d), and the symmetric bending motions near to  $450 \text{ cm}^{-1}$  [38] (Figure 7d). Furthermore, in the same figure, two peaks near  $900 \text{ cm}^{-1}$  probably belong to magnesium sulfate [39]. Finally, in Figure 6c, two characteristic bands of calcium sulfate [33] can be observed, approximately  $1600\text{--}1700 \text{ cm}^{-1}$ , mainly in JKCa2 and JKAll. In JKCa, there is one broad band ( $1630 \text{ cm}^{-1}$ ) characteristic of potassium jarosite, such as that showed in control spectra, supplemented so the results obtained in SEM (Figure 4a), where the growth of jarosite particles along the calcium sulfate can be observed.

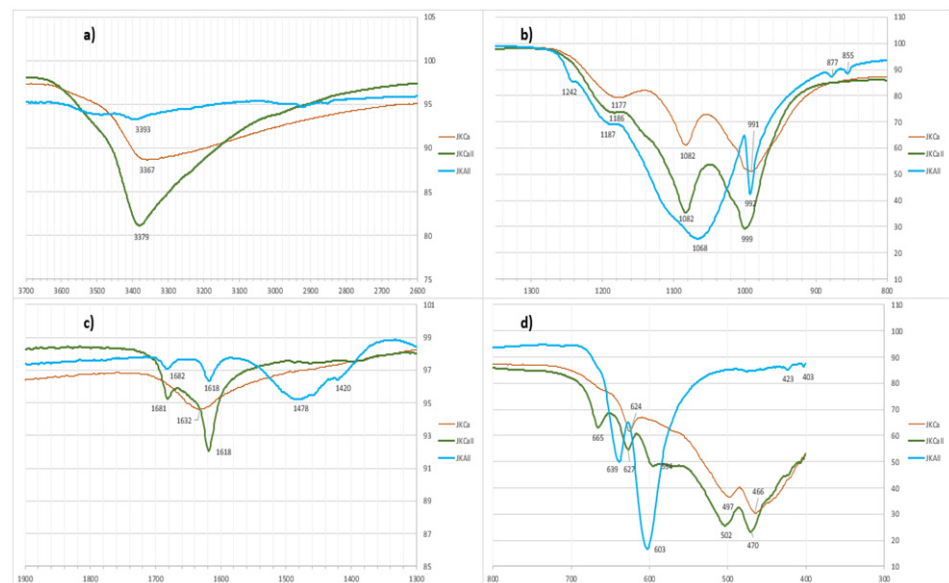


**Figure 7.** Comparative spectra obtained (a–d) for the corresponding doped jarosites obtained.

### 3.3. Mineralogical Characterization

Figure 8 shows the XRD results obtained for the doped jarosite-type compounds synthesized. It can be observed that for the sample of JKCa (Figure 8a), the typical pattern obtained is of the potassium jarosite but with a slight displacement to the left, which could be due to the expansion of the cell for the presence of calcium atoms into the jarosite structure (trigonal crystal system), confirming the doping with Ca.

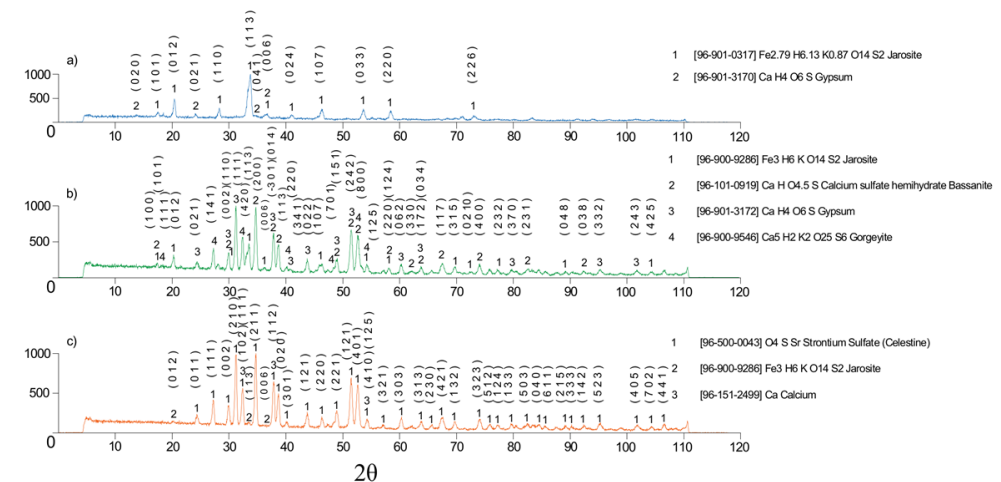


**Figure 8.** X-ray diffraction spectra for the doped jarosite-type compounds: (a) JKCa; (b) JKCa2; and (c) JKAl.

On the other hand, the sample JKCa2 shows a different spectrum (Figure 8b) from that to a potassium jarosite, showing a characteristic pattern of orthorhombic cell trigonal cells. Finally, a potassium jarosite phase in conjunction with another of calcium sulfate is found, as well as some peaks of calcium phases with sulfur overlapping and in the previously formed jarosite. Taking this into account, it could be considered that the addition of higher amounts of calcium (higher than stoichiometric) during synthesis can modify the crystal structure of jarosite.

For the case of JKAl (Figure 8c), it shows the X-ray diffraction spectrum where a similar spectrum to that shown in Figure 8b can be observed. In this case, the celestite phase of strontium sulfate can be identified as the corresponding phases for strontium

sulfate (celestite) and some peaks corresponding to the potassium jarosite. In this case, the XRD shows a change in the crystal structure from trigonal to orthorhombic, possibly due to the higher addition of doping elements during synthesis.

### 3.4. MTT Assay

Cell cytotoxicity results by MTT assays are shown in Figure 9. Cell viability increased significantly over time in both the control and jarosite groups. On day 3, the highest absorbance unit of metabolic activity was in cells in contact with JKAlI (23.63%  $\pm$  1.27%) and JKCa2 (17.83%  $\pm$  2.17%). The lowest absorbance unit of metabolic activity was in cells in contact with JKCa (16.23%  $\pm$  2.44%). On day 7, the highest metabolic activity was that of cells in contact with JKAlI (38.03%  $\pm$  4.38%), followed by cells in contact with JKCa2 (36.27%  $\pm$  5.37%). Again, the lowest absorbance unit of metabolic activity was in cells in contact with JKCa (29.60%  $\pm$  2.84%). Finally, on day 10, the metabolic activities did not increase much, being less than 50 absorbance units in the three jarosite samples compared to the control group (72.53  $\pm$  3.57), JKa2 (45.03%  $\pm$  5.1%), JKAlI (40.53%  $\pm$  6.81%) and JKCa (35.57%  $\pm$  7.1%).

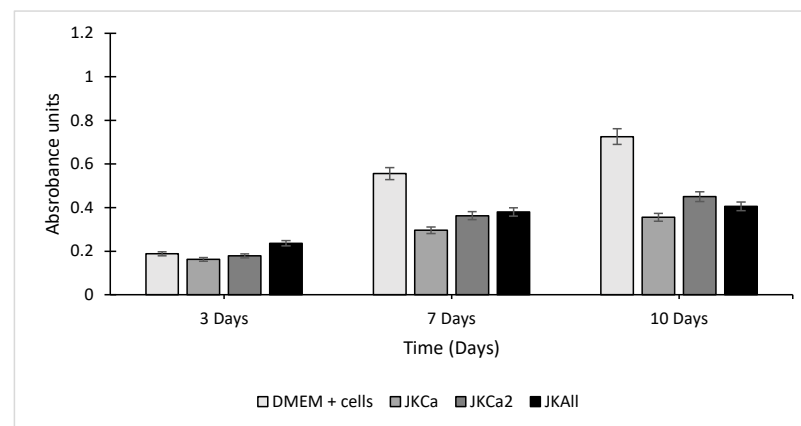


**Figure 9.** Cytotoxicity assay (MTT) of swine pulp cells seeded (4000 cell/well) with jarosite powders after 3, 7 and 10 days. Results are expressed as the mean and standard deviation of the cell viability.

### 3.5. Osteogenic Differentiation

Alizarin red staining can be used as an indicator of osteogenic differentiation [30]. After seeding the swine dental pulp stem cells in a 24-well plate, 10 mm<sup>3</sup> of jarosite powder (group b, c and e) was added. Figure 10b shows a few depositions of calcium that can be observed in the cells seeded in the JKCa2 + low-glucose DMEM (Bio-west, Mexico City), supplemented with 10% Fetal Bovine Serum (FBS) (Bio-west, Mexico City) and 1% penicillin-streptomycin (Sigma Aldrich, St. Louis, MO, USA). More evidence of the deposition of calcium can be observed in the cells seeded in the well of JKCa2 + MesenCult™ osteogenic differentiation (Figure 10c); a lot of deposition of calcium can be observed in the cells seeded in the well of JKAlI + low-glucose DMEM (Bio-west, Mexico City), supplemented with 10% Fetal Bovine Serum (FBS) (Bio-west, Mexico) and 1% penicillin-streptomycin (Sigma Aldrich, St. Louis, MO, USA) (Figure 10d); but a deep red of deposition of calcium can be observed in the cells seeded in the well of JKAlI + MesenCult™ osteogenic differentiation (Figure 10d); and finally, no evidence of deposition of calcium is observed in the control group (Figure 10a).

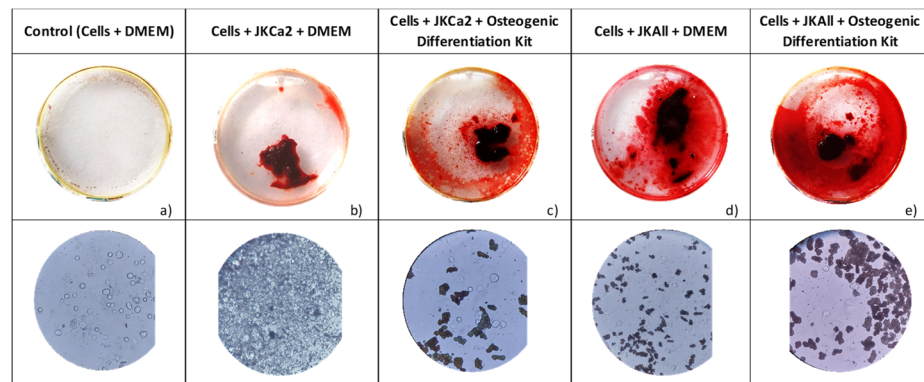


**Figure 10.** Representative images of the mineral deposition in swine dental pulp stem cells on day 21 by ARS, with their respective micrographs: (a) control (cells and DMEM); (b) cells, JKCa2 and DMEM; (c) cells, JKCa2 and osteogenic differentiation kit; (d) cells, JKAlI and DMEM; (e) cells, JKAlI and osteogenic differentiation kit.

## 4. Discussion

### 4.1. Chemical and Mineralogical Characterization

In Figure 11a, the crystalline structure of potassium jarosite (without doping) is shown, where there can be seen trigonal unit cells forming close-packed hexagonal structures. On the other hand, Figure 11b is a Ca doped potassium jarosite, where it is suggested that the migration of alkaline ions in the structures of JKCa is possible at high temperatures or is accompanied by a structural reorganization [18]. The above is consistent with the occurrence of the crystalline-amorphous transformation when an alkaline ion is inserted into the structure. It can also be seen that the intercalation of Ca ions during the first discharge occurs through a two-phase mechanism with the formation of the corresponding phase [40], obtaining a solid solution of JKCa modifying the unit cell and obtaining a combination between tetragonal and orthorhombic phases.

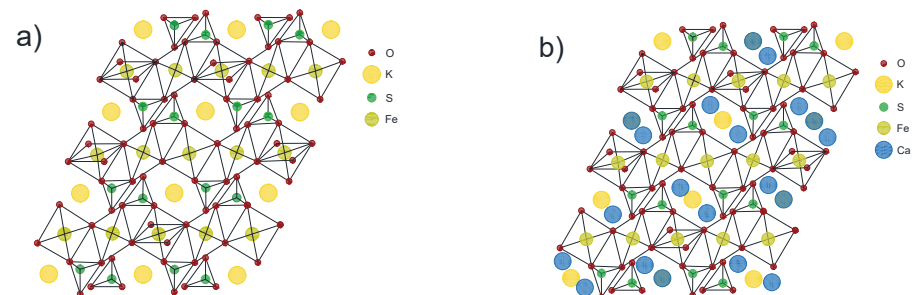


**Figure 11.** Representation of the crystalline structure of (a) the potassium jarosite, and (b) Ca doped potassium jarosite.

### 4.2. Cell Viability and Proliferation by MTT Assay

Previously, it was showed (Figure 9) the changes in relative cytotoxicity between swine dental pulp stem cells grown with JKCa, JKCa2, JKAlI and on the control group (no jarosite present). After day 3, JKCa had a cell viability and proliferation below JKCa2 and JKAlI in the three times evaluated, but when comparing JKCa2 and JKAlI, both had a very similar behavior on days 7 and 10, showing viable cells and increased cell proliferation as shown (Figure 9) by the cells' metabolism, according to ISO 10993-Part 5 [41]. It is possible that if we had evaluated at longer times the JKCa and JKAlI powders, for example, at 14 or 21 days, it would exceed 50% of viability and proliferation, since it is expressed in almost double the percentage increased from day 3 to day 10 in JKCa2, and JKAlI, as it was determined in other studies where the presence of Sr could improve the cell viability, osteogenic and angiogenic differentiation [42], and excellent bioactivity for bone regeneration besides an

excellent corrosion resistance [43]. Another explanation that can be visualized is to add less ( $7 \text{ mm}^3$  per well) powder quantity over the cells to allow a better stability of the cell culture, and they could migrate to the bottom of the plate allowing so more cells to live, and greater proliferation as shown in the control group without jarosite powder. This study is unique in that one exclusively investigated the single dose-dependent effects [44] of jarosite powder placed on swine dental pulp stem cells, looking specifically at cellular viability and proliferation.

To evaluate the osteoinductive property of the jarosite powders, we have chosen the ones that showed the best (JKCa2, JKAl) viability and proliferation with the MTT assay. In that sense, JKCa2 composition allowed osteoinduction when added to the swine dental pulp stem cells. Little coloration was observed on day 21, except for the JKAl composition shown and increased in deep red covering of almost the entire surface of the well, which shows that the composition of JKAl shows not only cells proliferation, for example, when they were cultured only with DMEM, which is evidenced by the presence of calcium, strontium and magnesium to demonstrate good osteoinductive properties.

## 5. Conclusions

The main target of this paper is related to the use of jarosite type-compounds as a biomaterial, but in this case this compound was doped with Ca, Sr and Mg to improve its cell viability and the osteogenic behavior. Doped potassium jarosite is viable for its use as a biomaterial, which is non-toxic, also allowing the proliferation of the cells at day 10 (Figure 9). Similarly, this compound is a possible osteoinductive material in the differentiation to the osteogenic lineage of swine pulp cells, given the results observed in Figure 10, having the presence of calcium deposits shown by Alizarin red staining at 28 days in the sample without inducing the medium. Its effectiveness could be improved by optimizing the amounts of powder used in the tests, as well as variations in its stoichiometry when synthesizing it.

Finally, it is important to point out that it is of special interest in the field of new technological discoveries applied to tissue engineering. Doped potassium jarosites with calcium, strontium and magnesium (JKCa, JKCa2 and JKAl) are promoted as cellularization, having also an important impact over cell differentiation, and osteogenesis of swine mesenchymal stem cells. It is feasible that these minerals joined with polymeric materials can be functionalized to produce scaffolds with osteoinductive properties and with the possibility of substituting culture media with cell differentiation properties.

**Author Contributions:** Conceptualization, E.S.-R., E.C.-S. and J.H.-Á.; methodology, E.S.-R., R.R.-I., J.R.S.-L. and A.M.G.-G.; validation, A.A.-F., M.d.P.G.-A. and M.A.V.-R.; formal analysis, E.S.-R. and R.R.-I.; investigation, E.S.-R., J.R.S.-L. and R.R.-I.; data curation, M.d.P.G.-A., M.A.V.-R. and A.A.-F.; writing—original draft preparation, J.R.S.-L., E.S.-R. and R.R.-I.; writing—review and editing, E.S.-R. and R.R.-I.; visualization, A.M.G.-G.; supervision, E.S.-R. and J.H.-Á.; project administration, E.S.-R. and R.R.-I. All authors have read and agreed to the published version of the manuscript.

**Funding:** This research received no external funding.

**Institutional Review Board Statement:** The animal study protocol was approved by the institutional Review Board of UNAM—FES Iztacala with the ethic approval number CE/FESI/052017/1174. Approved with date 09/05/2017.

**Informed Consent Statement:** Not Applicable.

**Data Availability Statement:** Data sharing is not applicable.

**Acknowledgments:** J. R. Serralde-Lealba (856653). Granted by CONACyT through the academic program of traditional doctorate in Materials Sciences (AUHS, Mexico). Thanks also goes to the Lab of Polymers of the AUHS, especially to Rosa A. Vázquez-García, Ana M. Herrera-González, Nayeli Trejo-Carbajal and Jesús García-Serrano.

**Conflicts of Interest:** The authors declare no conflict of interest.

## References

1. Dutrizac, J.E.; Kaiman, S. Synthesis and properties of jarosite type-compounds. *Can. Miner.* **1976**, *14*, 151–158. Available online: [https://rruff-2.geo.arizona.edu/uploads/CM14\\_151.pdf](https://rruff-2.geo.arizona.edu/uploads/CM14_151.pdf) (accessed on 28 April 2022).
2. Das, G.K.; Anand, S.; Achayra, S.; Das, R.P. Preparation and decomposition of ammoniumjarosite at elevated temperatures in  $\text{H}_2\text{O}(\text{NH}_4)_2\text{SO}_4\text{H}_2\text{O}$  media. *Hydrometallurgy* **1995**, *38*, 263–276. [[CrossRef](#)]
3. Drouet, C.; Navrotsky, A. Synthesis, characterization and thermo-chemistry of K-Na- $\text{H}_3\text{O}$  jarosites. *Geochim. Cosmochim. Acta* **2003**, *67*, 2063–2076. [[CrossRef](#)]
4. Smith, A.M.L.; Hodson-Edwards, K.A.; Dubbin, W.E.; Wright, K. Dissolution of jarosite  $[\text{KFe}_3(\text{SO}_4)_2(\text{OH})_6]$  at pH 2 and 8: Insights from batch experiments and computational modeling. *Geochem. Cosmochim. Acta.* **2006**, *70*, 608–621. [[CrossRef](#)]
5. Dutrizac, J.E. The behavior of the rare earths during the precipitation of sodium, potassium and lead jarosites. *Hydrometallurgy* **2004**, *73*, 11–30. [[CrossRef](#)]
6. Jarosites Crystals. Available online: [https://www.google.com/search?q=Jarosites+crystals&source=lnms&tbn=isch&sa=X&ved=2ahUKewjKwInRiYr4AhUMmmoFHXauD30Q\\_AUoAXoECAEQAw&biw=1920&bih=1057&dpr=1#imgrc=hrYNmSEEQKXrjM](https://www.google.com/search?q=Jarosites+crystals&source=lnms&tbn=isch&sa=X&ved=2ahUKewjKwInRiYr4AhUMmmoFHXauD30Q_AUoAXoECAEQAw&biw=1920&bih=1057&dpr=1#imgrc=hrYNmSEEQKXrjM) (accessed on 31 May 2022).
7. Hernández-Lazcano, E.; Cerecedo-Sáenz, E.; Hernández-Ávila, J.; Toro, N.; Karthik, T.V.K.; Mendoza-Anaya, D.; Fernández-García, M.E.; Rodríguez-Lugo, V.; Salinas-Rodríguez, E. Synthesis of Hydronium-Potassium Jarosite: Effect of pH and Aging Time on their Structural, Morphological and Electrical Properties. *Minerals* **2021**, *11*, 80. [[CrossRef](#)]
8. Long, D.T.; Fegan, N.E.; Mckee, J.D.; Lyons, W.B.; Macumber, P.G. Formation of alunite, jarosite and hydrous iron oxides in a hypersaline system: Lake Tyrrell, Victoria, Australia. *Chem. Geol.* **1992**, *96*, 183–202. [[CrossRef](#)]
9. Battler, M.M.; Osinski, G.R.; Lim, D.S.S.; Davila, A.F.; Michel, F.A.; Craig, M.A.; Izawa, M.R.M.; Leoni, L.; Slater, G.F.; Fairen, A.G.; et al. Characterization of the acidic cold sweep emplaced jarositic golden deposit, NWT, Canada, as an analogue for jarosite deposition on Mars. *Icarus* **2013**, *224*, 382–398. [[CrossRef](#)]
10. Varekamp, J.C.; Pasternack, G.B.; Rowe, G.L., Jr. Volcanic lake systematic II. Chemical constrains. *J. Volcanol. Geoth. Res.* **2000**, *97*, 161–179. [[CrossRef](#)]
11. Zolotov, M.Y.; Shock, E.L. Formation of jarosite-bearing deposits through aqueous oxidation of pyrite at Meridiani Planum, Mars. *Geophys. Res. Lett.* **2005**, *32*, L21203. [[CrossRef](#)]
12. Dutrizac, J.E.; Jambor, J.L. Jarosites and their application in hydrometallurgy. *Rev. Mineral. Geochem.* **2000**, *40*, 405–452. [[CrossRef](#)]
13. Salinas, E.; Roca, A.; Cruells, M.; Patiño, C.; Córdoba, D.A. Characterization and alkaline decomposition-cyanidation kinetics of industrial ammonium jarosite in NaOH media. *Hydrometallurgy* **2001**, *60*, 237–246. [[CrossRef](#)]
14. Xue, P.Y.; Ju, S.H.; Zhang, Y.F. Recovery of valuable metals by leaching of roasted jarosite residue. *Chin. J. Proc. Eng.* **2011**, *11*, 56–60.
15. Salinas, E.; Cerecedo, E.; Ramírez, M.; Patiño, F.; Pérez, M. Kinetics of alkaline decomposition and cyanidation of argentinian rubidium jarosite in NaOH medium. *Metall. Mater. Trans. B* **2012**, *43B*, 1027–1033. [[CrossRef](#)]
16. Perez-Labra, M.; Romero-Serrano, A.; Salinas-Rodríguez, E.; Avila-Davila, E.O.; Reyes-Perez, M. Synthesis, thermo chemistry and kinetics of alkaline decomposition of rubidium jarosite in  $\text{Ca}(\text{OH})_2$  media. *Metall. Mater. Trans. B* **2012**, *43B*, 773–780. [[CrossRef](#)]
17. Xu, E.; Xie, Z.; Cui, X.; Zhao, K.; Zhang, L.; Mai, L.; Wang, Y. Direct growth of an economic green energy storage material: A monocrystalline jarosite- $\text{KFe}_3(\text{SO}_4)_2(\text{OH})_6$ —Nanoplates@rGO hybrid as a superior lithium-ion battery cathode. *J. Mater. Chem.* **2016**, *10*, 3735–3742. [[CrossRef](#)]
18. Kosova, N.V.; Shindrov, A.A.; Kavanov, A.A. Theoretical and experimental study of reversible intercalation of Li ions in the Jarosite  $\text{NaFe}_3(\text{SO}_4)_2(\text{OH})_6$  structure. *Electrochem. Acta* **2020**, *359*, 136950. [[CrossRef](#)]
19. Chen, Z.; Liu, H.; Liu, X.; Cui, F.Z. Injectable calcium sulfate/mineralized collagen-based bone repair materials with regulable self-setting properties. *J. Biomed. Mater. Res. Part A* **2011**, *99A*, 554–563. [[CrossRef](#)]
20. Sidqui, M.; Collin, P.; Vitte, C.; Forest, N. Osteoblast adherence and resorption activity of isolated osteoclasts on calcium sulfate hemihydrate. *Biomaterials* **1995**, *16*, 1327–1332. [[CrossRef](#)]
21. Rosales, R.; Alvarado, K.; Ojeda, F. Ingeniería Tisular en Odontología. *ADM* **2012**, *69*, 164–167.
22. Lu, Z.; Wang, G.; Roohani-Esfahani, I.; Dunstan, C.R.; Zreiqat, H. Baghdadite ceramics modulate the cross talk between adipose stem cells and osteoblast for bone regeneration. *Tissue Eng. Part A* **2014**, *20*, 992–1002. [[CrossRef](#)] [[PubMed](#)]
23. Ramaswamy, Y.; Wu, C.; Van Hummel, A.; Combes, V.; Grau, G.; Zreiqat, H. The responses of osteoblast, osteoclast and endothelial cells to zirconium modified calcium-silicate-based ceramic. *Biomaterials* **2008**, *29*, 4392–4402. [[CrossRef](#)] [[PubMed](#)]
24. Haimi, S.; Moimas, L.; Pirhonen, E.; Lindroos, B.; Huhtala, H.; Rätty, S.; Kuokkanen, H.; Sándor, G.K.; Miettinen, S.; Suuronen, R. Calcium phosphate surface treatment of bioactive glass causes a delay in early osteogenic differentiation of adipose stem cells. *J. Biomed. Mater. Res. A* **2009**, *91*, 540–547. [[CrossRef](#)]
25. Mohan, B.G.; Suresh, B.S.; Varma, H.K.; John, A. In vitro evaluation of bioactive strontium-based ceramic with rabbit adipose-derived stem cells for bone tissue regeneration. *J. Mater. Sci. Mater. Med.* **2013**, *24*, 2831–2844. [[CrossRef](#)] [[PubMed](#)]
26. Yang, F.; Yang, D.; Tu, J.; Zheng, Q.; Cai, L.; Wang, L. Strontium enhances osteogenic differentiation of mesenchymal stem cells and in vivo bone formation by activating Wnt/catenin signaling. *Stem Cells* **2011**, *29*, 981–991. [[CrossRef](#)]
27. Azevedo, H.S.; Mata, A. Embracing complexity in biomaterials design. *Biomater. Biosyst.* **2022**, *6*, 100039. [[CrossRef](#)]
28. Van Meerloo, J.; Kaspers, G.J.; Cloos, J. Cell sensitivity assays: The MTT assay. *Methods Mol. Biol.* **2011**, *731*, 237–245. [[CrossRef](#)]

29. Puchtler, H.; Meloan, S.N.; Terry, M.S. On the history and mechanism of alizarin and alizarin red s stains for calcium. *J. Histochem. Cytochem.* **1969**, *17*, 110–124. [[CrossRef](#)]
30. Rosales-Ibáñez, R.; Cubo-Mateo, N.; Rodríguez-Navarrete, A.; González-González, A.M.; Villamar-Duque, T.E.; Flores-Sánchez, L.O.; Rodríguez-Lorenzo, L.M. Assessment of a PCL-3D printing-dental pulp stem cells triplet for bone engineering: An in vitro study. *Polymers* **2021**, *13*, 1154. [[CrossRef](#)]
31. Anderson, J.M.; Voskerician, G. The challenge of biocompatibility evaluation of Biocomposites. In *Biomedical Composites*, 1st ed.; Ambrosio, L., Ed.; Woodhead Publishing: Sawston, UK, 2010; pp. 325–352. ISBN 9781845694364. [[CrossRef](#)]
32. Settle, F.A. (Ed.) *Handbook of Instrumental Techniques for Analytical Chemistry*, 1st ed.; Prentice-Hall, Inc.: Upper Saddle River, NJ, USA, 1997; pp. 1–728.
33. Kamaraj, C.; Lakshmi, S.; Rose, C.; Muralidharan, C. Wet Blue Fiber and Lime from Leather Industry Solid Waste as Stabilizing Additive and Filler in Design of Stone Matrix Asphalt. *Asian J. Res. Soc. Sci. Hum.* **2017**, *7*, 240–257. [[CrossRef](#)]
34. Chemical Book—Strontium Sulfate. Available online: [https://www.chemicalbook.com/SpectrumEN\\_7759-02-6\\_IR1.htm](https://www.chemicalbook.com/SpectrumEN_7759-02-6_IR1.htm) (accessed on 6 June 2022).
35. Bishop, J.L.; Murad, E. The visible and infrared spectral properties of jarosite and alunite. *Am. Mineral.* **2005**, *90*, 1100–1107. [[CrossRef](#)]
36. Lane, M.D.; Christensen, P.R. Thermal Infrared Emission Spectroscopy of Salt Minerals Predicted for Mars. *Icarus* **1998**, *135*, 528–536. [[CrossRef](#)]
37. Vassallo, A.M.; Finnie, K.S. Infrared Emission Spectroscopy of Some Sulfate Minerals. *App. Spectro.* **1992**, *46*, 1477–1482. [[CrossRef](#)]
38. Herzberg, G., II. Infrared and Raman spectra of polyatomic molecules. In *Molecular Spectra and Molecular Structure*; Van Nostrand: New York, NY, USA, 1945; pp. 1–636.
39. Chemical Book—Magnesium Sulfate Heptahydrate. Available online: [https://www.chemicalbook.com/SpectrumEN\\_10034-99-8\\_IR1.htm](https://www.chemicalbook.com/SpectrumEN_10034-99-8_IR1.htm) (accessed on 6 June 2022).
40. Gnanavel, M.; Pralog, V.; Lebedev, O.M.; Caignaert, V.; Bazin, P.; Raveau, B. Lithium intercalation into the Jarosite-type hydroxysulfate: A topotactic reversible reaction from a crystalline phase to an inorganic polymer-like structure. *Chem. Mater.* **2014**, *26*, 4521–4527. [[CrossRef](#)]
41. ISO. Part 5—Use of International Standard ISO 10993-1, “Biological Evaluation of Medical Devices—Part 1: Evaluation and Testing within a Risk Management Process”. Available online: <https://www.fda.gov/media/85865/download> (accessed on 26 April 2022).
42. Wang, G.; Roohani-Esfahani, S.I.; Zhang, W.; Lv, K.; Yang, G.; Ding, D.; Zou, D.; Cui, D.; Zreiqat, Q.; Juang, X. Effects of Sr-HT-Gahnite on osteogenesis and angiogenesis by adipose derived stem cells for critical-sized calvarial defect repair. *Sci. Rep.* **2017**, *7*, 41135. [[CrossRef](#)]
43. Pham, D.Q.; Gangadoo, S.; Lu, Z.; Berndt, C.C.; Newsom, E.T.; Zreiqat, H.; Truong, V.K.; Ang, A.S.M. Strontium-doped hardystonite plasma sprayed coatings with robust antimicrobial activity. *Mater. Today Chem.* **2022**, *14*, 100822. [[CrossRef](#)]
44. Wang, J.; Witte, F.; Xi, T.; Zheng, Y.; Yang, K.; Yang, Y.; Zhao, D.; Meng, J.; Li, Y.; Li, W.; et al. Recommendation for modifying current cytotoxicity testing standards for biodegradable magnesium-based materials. *Acta Biomater.* **2015**, *21*, 237–249. [[CrossRef](#)]